4. Thick Chromium Atomic Force Microscopy Probes: Fabrication and Comparative Study

Hanna Konopacka[1], Hubert Grzywacz[1], Dariusz M. Jarząbek[1,2*]

[1] Faculty of Mechatronics, Institute of Micromechanics and Photonics, Warsaw University of Technology
Warsaw, Poland
[2] Institute of Fundamental Technological Research, Polish Academy of Sciences
Warsaw, Poland
[*] Corresponding Author: djarz@ippt.pan.pl

We present a report on the fabrication and characterization of chromium–nickel atomic force microscopy (AFM) probes with a chromium-coated tip and a bi-metallic cantilever. The introduction of a chromium layer enhances tip hardness and wear resistance, while nickel improves adhesion and reduces brittleness, enabling higher probe usability. The fabrication process was optimized through careful substrate polishing, photoresist selection, and stress control in chromium deposition, which limited the maximum chromium thickness to $\sim$1 µm. Mechanical testing confirmed that the probes operate reliably in AFM, achieving imaging quality comparable to commercial silicon probes, though resolution was constrained by the relatively large tip radius. Importantly, the design allows for tailoring of stiffness and resonance frequency by adjusting nickel thickness, broadening the applicability of the probes for both contact and intermittent-contact AFM modes. These results establish a proof-of-concept for durable metallic AFM probes engineered for tribological and high-load applications.
Keywords: atomic force microscopy (AFM), chromium–nickel probes, metallic cantilevers, probe fabrication, wear resistance, tip stiffness, tribological testing.

https://doi.org/10.24425/9788365550682.ch4

1. Introduction

Miniaturization is one of the major technological trends observed worldwide [1]. Along with smaller devices, such as micro-electro-mechanical systems

MEMS [2], there comes a need for a more sophisticated understanding of micro- and nano-scale behaviour. Such understanding should provide the ability to anticipate device failure. One of the approaches for small-scale material characterization is Atomic Force Microscopy AFM, in use since 1986 [3]. The most common setup includes a silicon probe, which proved to be useful for a high number of applications [4]. However, one should be aware that some problems depend on mutual interactions between the sample and probe. Thus, the material of the probe's tip should be chosen based on the requirements of a given application. Examples where this is a crucial aspect of the experiment design are: friction coefficient measurement [5, 6], adhesion [5, 6], and wear [7]. Notably, yet another issue is the experimental range of such parameters as the maximum force or resonance frequency of the AFM probe. A method that provides a broadening of the range of materials, stiffness, and tip shapes was shown in [8]. So far, it has been used for preparing an all-metal cantilever, but made from a single element. Augmenting this approach for a two-elemental system may have benefits such as higher stiffness, better adhesion of consequent layers of metal as well as increased hardness of the tip.

In this work, we showed an improved use of the abovementioned approach to provide a chromium tip with a chromium-nickel cantilever. A chromium tip has been chosen to further improve the wear resistance of the apex of the tip. The chromium-nickel cantilever has been designed for higher stiffness than the pure nickel cantilever. The addition of nickel also reduced brittleness, thereby increasing usability. The main result of this work is the successful fabrication of a chromium-tip, chromium-nickel cantilever AFM probe and its proof-of-concept in a simple tribological test.

2. Experimental

2.1. Probes design

One of the main advantages of the all-metal probes is a possibility to design a cantilever for a specific stiffness. A nominal stiffness and resonance frequency for given cantilever dimensions were calculated as follows:

– Effective Young's modulus E_{eff} for bi-material cantilever:

$$E_{\text{eff}} = \frac{E_{\text{Ni}} \cdot I_{\text{Ni}} + E_{\text{Cr}} \cdot I_{\text{Cr}}}{I_{\text{tot}}}, \tag{1}$$

where E_{Ni} and E_{Cr} are Young's moduli of Ni and Cr, respectively, and I_{Ni}, I_{Cr}, and I_{tot} are moments of inertia of Ni part of the cross-section, Cr part of the cross section, and the total cross-section of the cantilever. The geometry of the cantilever is defined as shown in Fig. 1.

– The effective density ρ_{eff} for a bi-material cantilever:

$$\rho_{\text{eff}} = \frac{\rho_{\text{Ni}} \cdot V_{\text{Ni}} + \rho_{\text{Cr}} \cdot V_{\text{Cr}}}{V_{\text{tot}}}, \tag{2}$$

where ρ_{Ni} and ρ_{Cr} are densities of Ni and Cr, respectively, and V_{Ni}, V_{Cr}, and V_{tot} are volumes of Ni part, Cr part, and the total of cantilever.

– Theoretical stiffness k_{eff} and resonance frequency $\omega_{0\text{eff}}$:

$$k_{\text{eff}} = \frac{E_{\text{eff}} \cdot b \cdot h^3}{4 \cdot L^3}, \tag{3}$$

$$\omega_{0\text{eff}} = \frac{\lambda_0^2}{2\sqrt{3}} \cdot \sqrt{\frac{E_{\text{eff}}}{\rho_{\text{eff}}}} \cdot \frac{h}{L^2} \cdot \frac{1}{2\pi}, \tag{4}$$

where λ_0 – constant equal to $0.596864 \cdot \pi$.

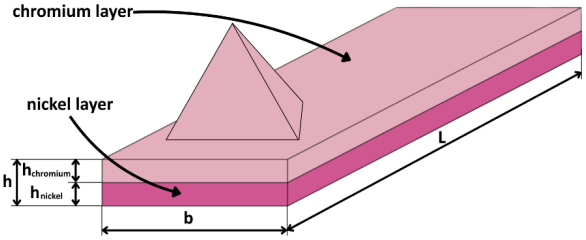

Fig. 1. Geometry of the designed chromium–nickel cantilever with chromium coating on the tip. Dimensions used for stiffness and resonance frequency calculations are indicated.

The Young modulus and theoretical density are determined by the choice of materials; however, the fabrication design can influence k_{eff} and $\omega_{0\text{eff}}$ through the cantilever geometry. As shown in Table 1, an appropriate choice of dimensions enables the design of probes suitable for both contact and intermittent-contact AFM modes. The calculations were performed for a fixed cantilever length of 450 µm and a chromium layer thickness of 1 µm.

2.2. Probes fabrication

An experimental fabrication process was conducted as shown in Fig. 2.

In step 1, a sacrificial substrate is polished to a mirror finish. Step 2 is indenting the substrate to prepare a mold for the cantilever's tip. Step 3 consists of photoresist deposition on the substrate with dimensions equal to the dimensions of the cantilever and its base. Step 4 is an electrodeposition of Cr for a designed thickness with subsequent deposition of nickel, aiming for a designed total thickness. One should note that after this step, a tip is prepared from nickel as well

Table 1. Calculated stiffness and resonance frequency of chromium–nickel cantilevers for various nickel thicknesses and widths (chromium layer thickness fixed at 1 µm).

For the chromium–nickel cantilever			
Width b [µm]	Nickel thickness h [µm]	Stiffness k [N/m]	Resonance frequency ω_0 [kHz]
20	0.25	0.028	5.895
50	0.25	0.071	5.895
200	0.25	0.282	5.895
20	0.5	0.047	6.828
50	0.5	0.117	6.828
200	0.5	0.468	6.828
20	0.75	0.072	7.765
50	0.75	0.18	7.765
200	0.75	0.721	7.765
20	1	0.105	8.705
50	1	0.263	8.705
200	1	1.051	8.705
20	2	0.335	12.475
50	2	0.838	12.475
200	2	3.353	12.475
20	5	2.526	23.809
50	5	6.316	23.809
200	5	25.264	23.809
20	10	15.131	42.712
50	10	37.827	42.712
200	10	151.308	42.712

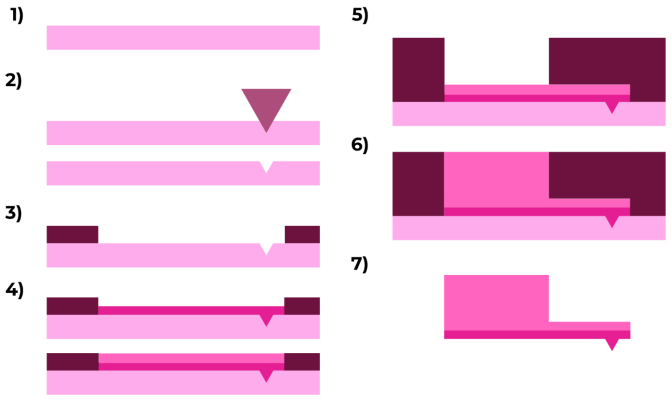

Fig. 2. Schematic of the fabrication process: (1) substrate polishing, (2) tip mold preparation by indentation, (3) photoresist deposition, (4) chromium and nickel electrodeposition, (5) mold preparation for base, (6) nickel deposition of base, (7) substrate removal.

as the whole Cr-Ni cantilever. The following steps include: 5 – preparing a thick photoresist layer as a mold for a cantilever base; 6 – electrodeposition of nickel to fill that mold. Finally, step 7 is etching a sacrificial substrate to reveal the tip, cantilever and base.

This approach resulted in a tip with increased hardness, better adhesion of the first (Cr) layer to the second (Ni) layer than for the Ni–Ni interface, and higher stiffness. For chrome deposition, Chrome Plating Solution (dr Galva, Germany) with the following parameters: temperature = 25 °C, voltage = 3 V, current density = 24 A/dm2, and time = 220 s. Initially, the rest of the parameters were the same as in [8]. However, for improving the quality of the fabricated cantilevers, the process was optimized and a comparison of initial and final results will be shown as well as the final fabrication process.

3. Probes testing

Probes were tested after each fabrication step with optical microscopy (DSX 500, Olympus, Japan) or scanning electron microscopy (Zeiss Crossbeam 350, Zeiss, Germany). For performance testing of the ready-to-use probe, AFM (Flex-AFM, Nanosurf, Switzerland) was used. Comparison with the commercially available HQ:CSC17/Al BS (MikroMasch, USA) silicon probe was carried out on the O-doped NbN sample. AFM data were treated in the Gwyddion open-source software.

4. Results

4.1. Polishing

The substrate roughness is a direct predictor of the roughness of the as-deposited metal. The first deposited layer (step 4 in Fig. 2) forms the backside

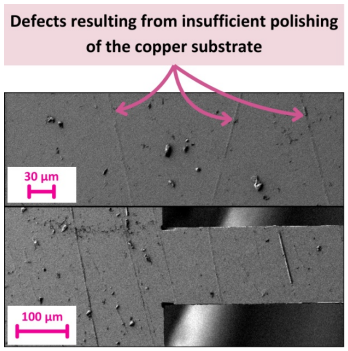

Fig. 3. Polished substrate surface. Smoother finish ensures reduced cantilever backside roughness and improved AFM laser reflection.

of the cantilever, which reflects the laser beam. Therefore, low surface roughness *Sa* is required to ensure a high-quality laser signal. However, since *Ra* and *Sa* are statistical parameters, they may not fully capture local surface imperfections. Inadequate polishing of the substrate can lead to residual material irregularities, which are then reproduced in the deposited layers. Such imperfections, if located near the tip mold on the front side of the cantilever (step 2 in Fig. 2), may strongly deteriorate the probe quality. For this reason, each cantilever is inspected for polishing-related defects, as shown in Fig. 3.

5. Photoresist

One of the crucial steps of the fabrication of metal probes is the photoresist deposition of the substrate. Details of this process are shown in Fig. 4.

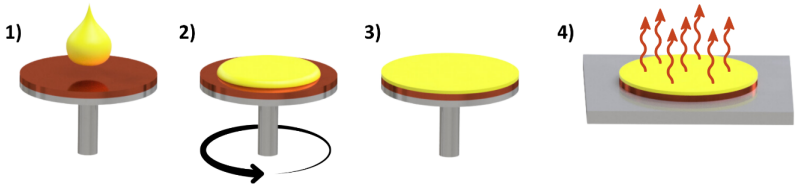

Fig. 4. Process of photoresist deposition: 1) droplet application on the substrate, 2, 3) spin-coating for uniform distribution, and 4) soft-baking for stabilization of the layer.

In step 1 photoresist droplet is deposited on the substrate. Step 2 is centrifuging this droplet by rotating the substrate. As the smooth layer of photoresist covers the substrate, in the final step, the whole system is soft-baked for 1 min at 80 °C and then for 15 min at 135 °C. The rotation speed was selected according to the photoresist thickness characteristics provided by the manufacturer and was set to 1500 rpm, which resulted in a layer thickness of 50 µm. With this result, the photoresist thickness can be chosen according to the desirable cantilever thickness.

Yet another issue connected with photoresist is its chemical resistivity. In the earlier work, it was shown that AZ 15nXT photoresist can be readily used with a Ni electrodeposition bath as a suitable mask. Preliminary tests with Cr electrodeposition bath showed that this photoresist is highly deteriorated during the process (Fig. 5a). Chemically resistant AZ125-10B was used, both without (Fig. 5b) and with additional baking (Fig. 5c). Results for Cr structures are shown in Fig. 5.

Changing the photoresist to AZ125-10B as well as applying additional baking led to a significant increase in the quality of electrodeposited Cr structures. This allows this process to be used to fabricate cantilevers. Fabrication of the third photoresist layer for AFM probes presents several challenges. Substrate preparation takes about an hour, and exposure can last up to thirteen hours,

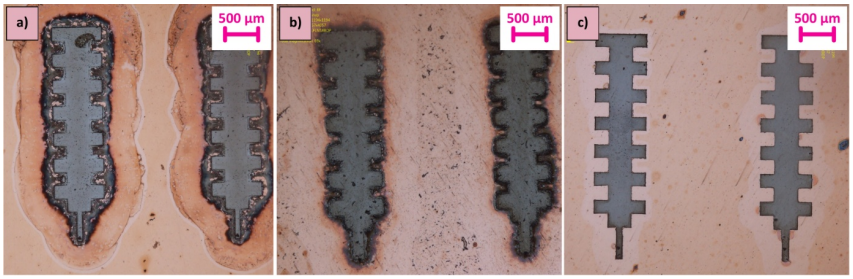

Fig. 5. Effect of photoresist selection during chromium electrodeposition: a) AZ 15nXT degraded, b) AZ125-10B stable, c) AZ125-10B with additional baking. The optimized process yielded high-quality chromium layers.

making it difficult to maintain stable environmental conditions. Variations in temperature and humidity lead to uneven resist thickness and defects. Selecting the correct exposure energy is critical: too low energy results in incomplete cross-linking, while too high energy can cause cracking or stress.

Common failure modes include (Fig. 6): a) electrolyte penetration beneath the photoresist, which can be minimized by proper exposure energy; b) pho-

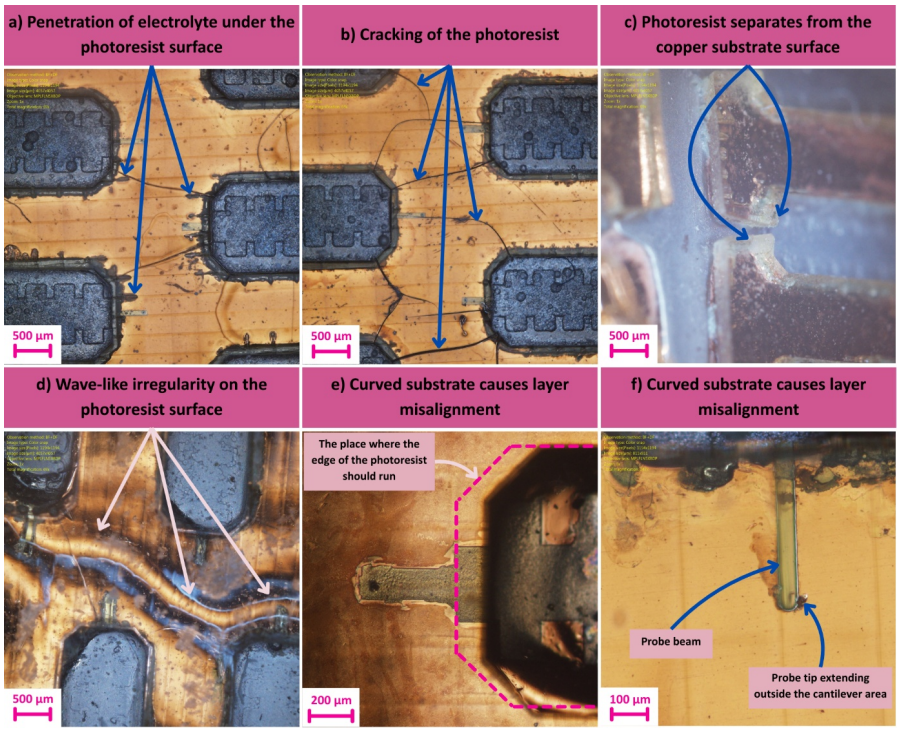

Fig. 6. Example of photoresist defects observed during fabrication of the third photoresist layer for AFM probes.

toresist cracking, controlled by adjusting the exposure dose; c) photoresist separation from the copper substrate, prevented by thorough surface cleaning and optimized exposure; d) wave-like surface irregularities, reduced by selecting the appropriate resist thickness and exposure parameters; e) substrate warping causing layer misalignment, addressed through careful attachment before polishing; and f) substrate warping causing layer misalignment, addressed through careful detachment after polishing.

Even minor defects in the mask can significantly affect probe geometry, making precise control of the process essential.

6. Tip-mold

Typically, the indentation impression perfectly resembles the indentation tip shape as well as other indentation-related phenomena. This leads to the visible re-creation of a pile-up pattern of the deposited metal, as shown in Fig. 7a.

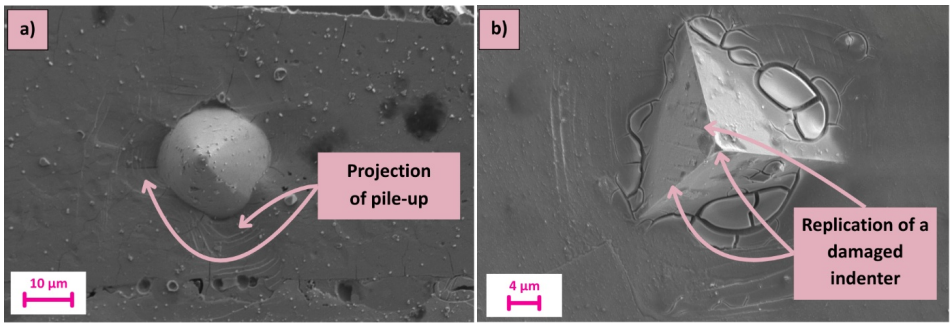

Fig. 7. Tip defects resulting from a blunted indenter during mold preparation.

This effect may be mitigated by lowering the indentation force as well as changing the indenter shape. However, it should be noted that pile-ups are significantly lower than the height of the nominal impression. Another reason for inspecting the tip of as-received cantilever is indentation tip blunting. The result of damaged indentation tip on the cantilever's tip is shown in Fig. 7b.

It can be seen that the very apex of the tip is of irregular shape. It means that the indentation tip for tip molding should be renewed. Yet another possible issue with tip molding is residual photoresist in the mold before metal deposition, as described in Fig. 8.

This problem occurred when the removal of untreated photoresist was too fast. Successful removal of the photoresist from the bottom of the 15 µm tip impression was achieved by using an acetone bath in an ultrasonic cleaner for 15 minutes.

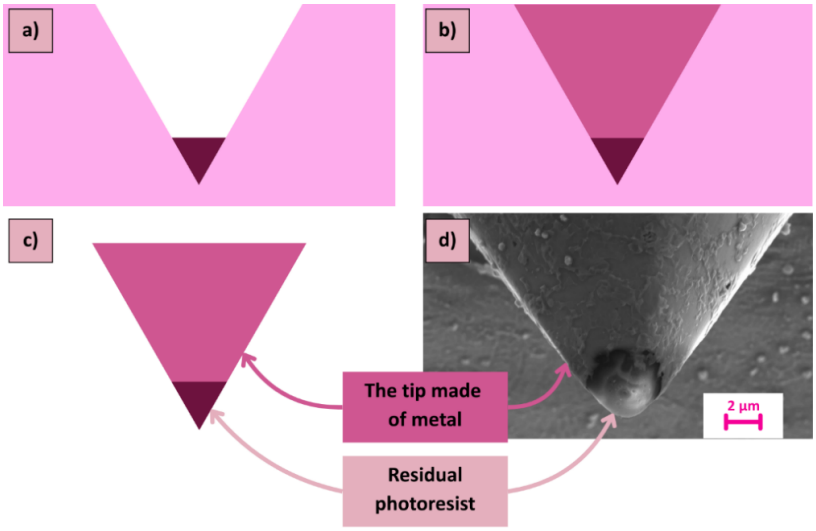

Fig. 8. Tip-mold defects caused by residual photoresist: a) photoresist remaining in the mold, b) metal electrodeposition with residual resist trapped at the bottom of the mold, c) after substrate etching the residual resist formed the tip instead of metal, d) optical image of a probe with residual photoresist on the tip.

7. Bi-layer cantilever

Initially, we intended to fabricate cantilevers with a wide range of Cr and Ni thicknesses ratio. However, Cr coating with a thickness over 1 µm proved to be highly internally stressed, as shown in Fig. 9.

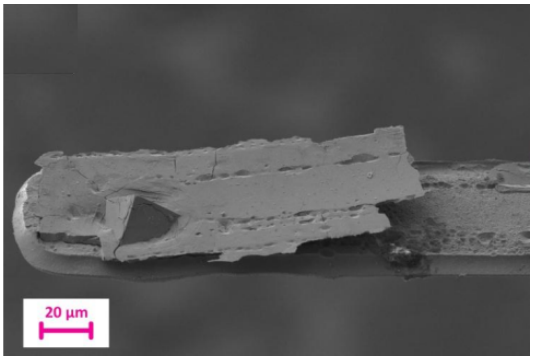

Fig. 9. Scanning electron micrograph of chromium–nickel cantilever showing intact bilayer structure with chromium thickness limited to ∼1 µm to prevent delamination.

Such stresses led to the detachment of the Cr layer from Ni the layer. Restricting the fabrication process to the Cr layer not thicker than 1 µm led to

intact cantilevers. However, those cantilevers should also meet other requirements. The most basic function of the cantilever is to apply a normal force for tip-sample interaction. Being able to control that process means that back-side of the cantilever has to reflect the laser beam into the four-quadrant diode. This can happen only for a sufficiently smooth surface. In Fig. 10, the OM images of the nickel surface of the back-side of the cantilever are shown in the as-deposited state as well as after mechanical polishing.

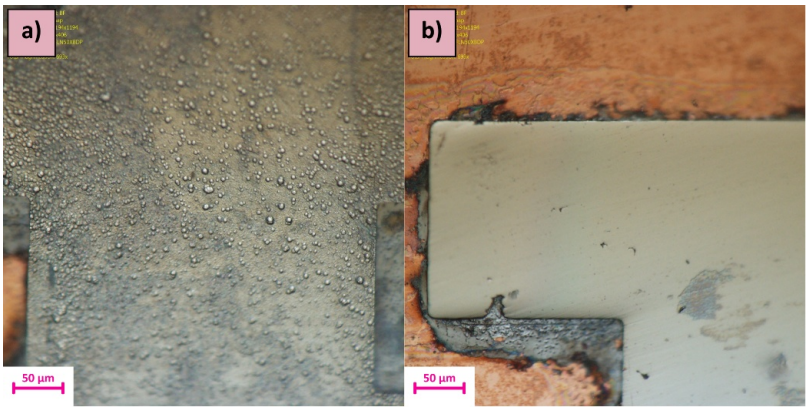

Fig. 10. Optical micrographs of nickel cantilever backside: a) as-deposited surface with high roughness, b) polished surface enabling laser reflection.

Adding a polishing step is an important change compared to the original process flow. Here, the surface roughness of as-deposited Ni on Cr was significantly higher than for all-Ni cantilevers. Mechanical polishing was carried out with 1 µm diamond suspension. Such an approach led to slow material removal, which provided control over the resulting thickness of deposited Ni as well as the small roughness needed for laser reflection.

8. Cantilever testing

With the successful fabrication of Cr-Ni AFM probes, mechanical testing in AFM was carried out. The probe used for those tests is shown in Fig. 11.

Measurements were carried out with the fabricated chromium–nickel probe using a Nanosurf Flex AFM, as shown in Fig. 12a, while Fig. 12b presents a reference measurement obtained with a commercial silicon probe. Although the images acquired with the chromium–nickel probe are not of the highest resolution, they remain comparable to those obtained with silicon probes. This limitation is mainly attributed to the relatively large tip radius of the fabricated probe.

The result of roughness *Sa* on the O-doped NbN sample for both Si and Cr-Ni AFM probes is shown in Fig. 13.

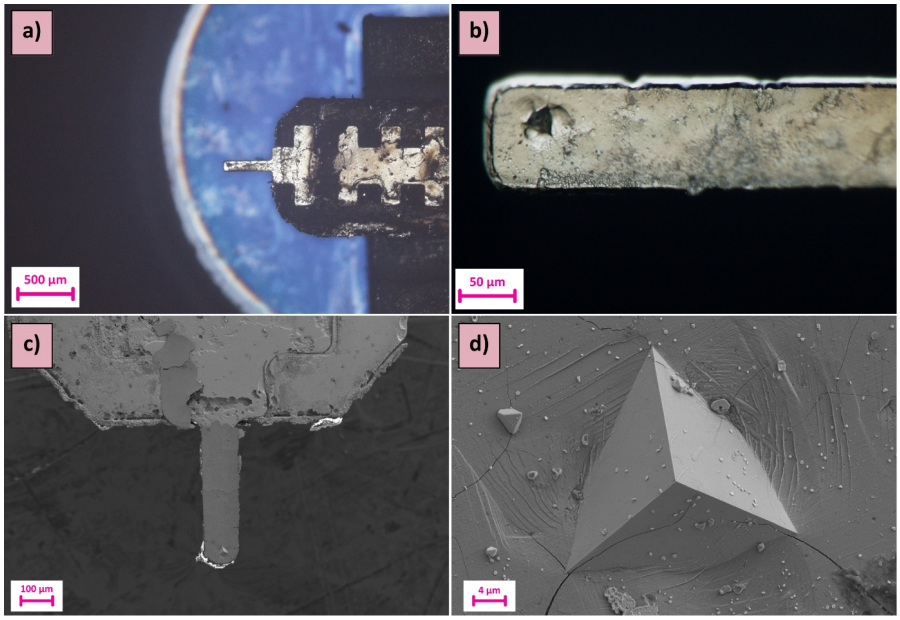

Fig. 11. Images of fabricated chromium–nickel probes: a, b) optical microscope images of completed probes, and c, d) scanning electron microscopy (SEM) images of fabricated probes.

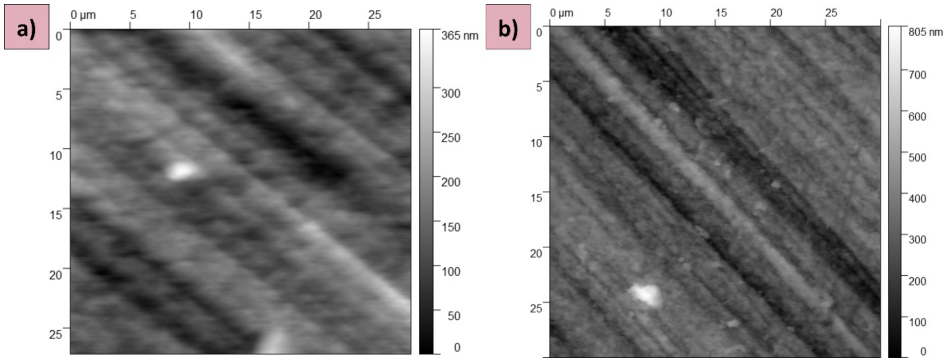

Fig. 12. AFM measurements of O-doped NbN sample: a) acquired using the fabricated chromium–nickel probe, b) reference measurement obtained with a commercial silicon probe.

Statistical analysis of the surface roughness measurements yielded a mean $Sa = 94.2 \pm 27.8\,\text{nm}$ for the chromium–nickel probe and $Sa = 65.3 \pm 1.2\,\text{nm}$ for the silicon probe ($n = 63$ and $n = 66$, respectively). While the chromium–nickel probe exhibited a higher measurement dispersion, this behavior reflects its increased stiffness and robustness, which makes it suitable for high-load and tribological AFM applications. Despite the larger tip radius, the chromium–nickel probe provided imaging quality comparable to the silicon probe and demon-

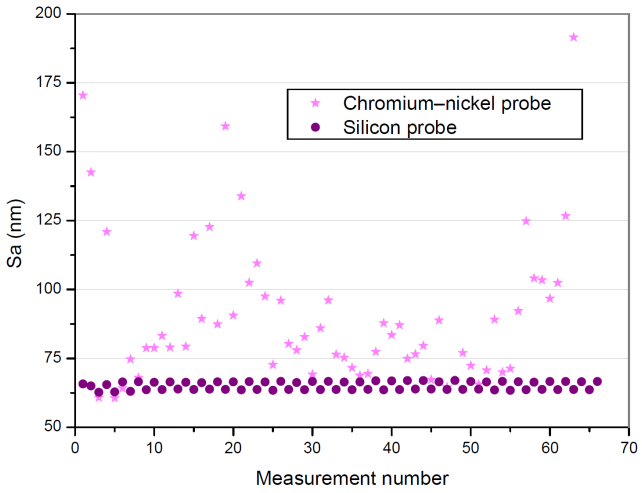

Fig. 13. Comparison of surface roughness (Sa) values measured on O-doped NbN sample using chromium–nickel probe and commercial silicon probe.

strated mechanical durability which enables stable operation under demanding measurement conditions.

9. Discussion

The fabrication of chromium–nickel AFM probes presented here demonstrates both the feasibility and challenges of extending bi-metallic approaches to the AFM probe design. The introduction of a chromium layer at the tip region improved wear resistance, while the nickel underlayer mitigated brittleness and facilitated adhesion between layers. Nevertheless, several fabrication challenges were encountered, particularly stress accumulation in thick chromium coatings. These stresses limited the maximum practical chromium thickness to approximately 1 µm, which constrained the design space. The necessity of additional polishing steps further underscores the sensitivity of the optical readout to surface roughness, highlighting that the introduction of chromium requires process modifications compared with all-nickel probes.

The successful operation of chromium–nickel probes in AFM measurements confirmed that they can reach imaging quality comparable to that of commercial silicon probes. While the resolution was limited by the relatively large tip radius, the tribological benefits of chromium – particularly hardness and wear resistance – are expected to enhance probe longevity in demanding applications. The fabrication approach also demonstrated flexibility: by tuning nickel thickness, a wide range of cantilever stiffness values and resonance frequencies can

be achieved, offering opportunities for tailoring probes to specific experimental requirements. However, scaling the process and ensuring reproducibility remain open issues. Variability in photoresist stability, substrate preparation, and tip-mold definition will need to be systematically addressed before the probes can become competitive alternatives in routine AFM applications.

10. Conclusions

We have demonstrated a chromium–nickel AFM probe architecture that combines a chromium tip with a nickel-supported cantilever. This design improves hardness, adhesion and stiffness while maintaining functional imaging capability comparable to silicon probes. Although fabrication challenges – particularly stress management in chromium layers – currently limit process robustness, the concept opens a pathway towards durable metallic probes tailored for high-load and tribological AFM experiments. Future refinements in tip shaping and stress control should enable probes with both higher resolution and enhanced longevity, broadening the experimental scope of AFM in materials science and nanotechnology.

Although the fabricated Cr–Ni probes exhibited slightly higher roughness dispersion compared to commercial silicon probes, their durability and resistance to wear make them promising for high-load or tribological AFM applications.

Acknowledgements

This research was supported by the National Centre for Research and Development (Poland) grant TANGO-IV-B/0002/2019.

References

1. Pattanaik P., Ojha M., Review on challenges in MEMS technology, *Materials Today: Proceedings*, **81**(Part 2): 224–26, 2023, https://doi.org/10.1016/j.matpr.2021.03.142.
2. Yellampalli S. [Ed.], *MEMS Sensors: Design and Application*, IntechOpen, 2018, https://doi.org/10.5772/intechopen.71153.
3. Binnig G., Quate C.F., Gerber Ch., Atomic force microscope, *Physical Review Letters*, **56**(9): 930–933, 1986, https://doi.org/10.1103/PhysRevLett.56.930.
4. Voigtländer B., *Atomic Force Microscopy*, 2nd ed., Springer Nature, Cham, 2019, https://doi.org/10.1007/978-3-030-13654-3.
5. Bhushan B. [Ed.], *Nanotribology and Nanomechanics: An Introduction*, 4th ed., Springer International Publishing, Cham, 2017, https://doi.org/10.1007/978-3-319-51433-8.

6. Butt H.-J., Cappella B., Kappl M., Force measurements with the atomic force microscope: Technique, interpretation and applications, *Surface Science Reports*, **59**(1–6): 1–152, 2005, https://doi.org/10.1016/j.surfrep.2005.08.003.

7. Gnecco E., Meyer E., *Fundamentals of Friction and Wear on the Nanoscale*, 2nd ed., Springer International Publishing, Cham, 2024.

8. Milczarek M., Jarząbek D.M., Jenczyk P., Bochenek K., Filipiak M., Novel paradigm in AFM probe fabrication: Broadened range of stiffness, materials, and tip shapes, *Tribology International*, **180**: 108308, 2023, https://doi.org/10.1016/j.triboint.2023.108308.